processes

MDPI

Article

A Novel Optimal Planning and Operation of Smart Cities by Simultaneously Considering Electric Vehicles, Photovoltaics, Heat Pumps, and Batteries

Masoud Shokri [1,2], Taher Niknam [1,*], Miad Sarvarizade-Kouhpaye [3], Motahareh Pourbehzadi [4], Giti Javidi [4], Ehsan Sheybani [4,*] and Moslem Dehghani [1]

[1] Department of Electrical and Electronics Engineering, Shiraz University of Technology, Shiraz 7155713876, Iran; m.shokri8168@yahoo.com (M.S.); mo.dehghani@sutech.ac.ir (M.D.)
[2] Fars Regional Electric Company, Shiraz 7134696333, Iran
[3] Institute for Research in Technology (IIT), School of Engineering (ICAI), Comillas Pontifical University, 28015 Madrid, Spain; msarvarizadeh@comillas.edu
[4] School of Information Systems and Management, Muma College of Business, University of South Florida, Tampa, FL 33620, USA; mpourbehzadi@usf.edu (M.P.); javidi@usf.edu (G.J.)
* Correspondence: niknam@sutech.ac.ir (T.N.); sheybani@usf.edu (E.S.)

Abstract: A smart city (SC) includes different systems that are highly interconnected. Transportation and energy systems are two of the most important ones that must be operated and planned in a coordinated framework. In this paper, with the complete implementation of the SC, the performance of each of the network elements has been fully analyzed; hence, a nonlinear model has been presented to solve the operation and planning of the SC model. In the literature, water treatment issues, as well as energy hubs, subway systems (SWSs), and transportation systems have been investigated independently and separately. A new method of subway and electric vehicle (EV) interaction has resulted from stored energy obtained from subway braking and EV parking. Hence, considering an SC that simultaneously includes renewable energy, transportation systems such as the subway and EVs, as well as the energy required for water purification and energy hubs, is a new and unsolved challenge. In order to solve the problem, in this paper, by presenting a new system of the SC, the necessary planning to minimize the cost of the system is presented. This model includes an SWS along with plug-in EVs (PEVs) and different distributed energy resources (DERs) such as Photovoltaics (PVs), Heat Pumps (HPs), and stationary batteries. An improved grey wolf optimizer has been utilized to solve the nonlinear optimization problem. Moreover, four scenarios have been evaluated to assess the impact of the interconnection between SWSs and PEVs and the presence of DER technologies in the system. Finally, results were obtained and analyzed to determine the benefits of the proposed model and the solution algorithm.

Keywords: grey wolf optimization algorithm; optimal planning and operation; regenerative braking energy; smart city

Citation: Shokri, M.; Niknam, T.; Sarvarizade-Kouhpaye, M.; Pourbehzadi, M.; Javidi, G.; Sheybani, E.; Dehghani, M. A Novel Optimal Planning and Operation of Smart Cities by Simultaneously Considering Electric Vehicles, Photovoltaics, Heat Pumps, and Batteries. *Processes* **2024**, *12*, 1816. https://doi.org/10.3390/pr12091816

Academic Editor: Jiaqiang E

Received: 6 July 2024
Revised: 12 August 2024
Accepted: 20 August 2024
Published: 27 August 2024

1. Introduction

Urban areas have been dealing with various challenges. These challenges include sustainable development, enhancing services provided to citizens, reducing carbon generation, decreasing emissions of pollutants, and improving the utilization of resources. These challenges have drawn attention to more efficient energy management (EM) within urban areas. A smart city (SC) is a concept developed to achieve a more energy-efficient urban area [1]. A comprehensive scheme of an SC considers the entire energy systems presented in the model. This includes transportation systems such as plug-in electric vehicles (PEVs) and subway systems (SWSs), and distributed energy systems such as Photovoltaics (PVs),

Heat Pumps (HPs), and batteries. Considering the interconnection and cooperative operation of various energy systems within the SC model causes the model to become more energy-efficient and flexible in supplying the total demands of the system.

Creating sustainable and better-functioning transportation systems is among the main goals of smart cities [2]. High air pollution and traffic congestion are the main challenges facing urban transportation systems [3]. Hence, a more efficient, secure, and eco-friendly transport system is highly valued for the design of present and future cities. Transportation systems are among the major consumers of energy, and smart management of them is of great importance in lowering the energy consumption of the SC model. The interconnections between all different parts, including the transportation systems and distributed energy systems, must be modeled to obtain a more comprehensive and efficient SC model.

PEVs and subways (SWs) are among the most utilized parts of the transportation systems in cities. PEVs constitute 5% of the loads in an electric grid [3,4]. Therefore, they need to be managed efficiently in order to obtain a sustainable SC model. PEVs can also be used as a distributed resource for the grid when they are parked in a parking lot and are being discharged. A handful of researchers have focused on the optimal management of PEVs and the challenges they add to the model. In [5], an optimized bidirectional vehicle-to-grid (V2G) system operation is presented that carries out the day-ahead scheduling of PEVs' charging/discharging. An adaptive control method to manage PEV charging/discharging for load leveling and peak shaving is presented in [6]. Ref [7] presents a novel EM scheme for optimal integration of PEVs into a distribution system that involves two layers for active and reactive power management. The SWS is the other major component of the transportation system. Consequently, many researchers have studied SWSs and assessed their impact on different parts of the entire system, and different studies are considered as approaches to improve the efficiency of urban SWSs. Regenerative braking energy (RBE) is considered to be a solution for the efficient EM of SWSs. In [8], a timetable optimization method was proposed to utilize the braking energy (BE). This method is based on adjusting the departure and arrival time of trains to use the BE of the arriving train directly from the train that is leaving. Another method utilizes energy storage systems (ESSs) to reserve the BE for later consumption. A novel method combining timetable optimization and onboard ESS utilization was proposed in [9]. Wayside placement of an ESS is an alternative way of implementing an ESS in urban SWSs. In [10], a wayside ESS and its different ways of connecting to the system, including connection via the bidirectional converters and direct connection, are studied. Another method employs reversible substations to feed the RBE back to the upstream AC grid [11].

Different types of distributed energy resources (DERs) are incorporated into the SC model to benefit from their advantages toward a more efficient SC. Stationary batteries can be utilized for EM by storing electricity at off-peak hours and decreasing purchased power from the grid. Air pollutants and greenhouse gasses are among the most noticeable challenges of modern society. PVs are extensively utilized in residential, commercial, and industrial sectors to convert light energy into electricity and reduce air pollutants [12]. Finally, electrification of heating by utilizing HPs along with renewable power generation is recognized as an important factor in reducing carbon dioxide in the process of supplying heat [13]. Considering these factors leads to the motivation of incorporating DERs into the SC model.

As stated above, the interconnection between PEVs, metro systems, and DERs in the SC must be considered to attain a more realistic and efficient EM in the SC model. The following papers are some examples of the research conducted in this regard. A programming model is used to investigate the synergy between DERs and transportation systems in the context of an SC [14]. However, the proposed model is a simple linear model and the investigated scenarios are limited. In addition, the destruction cost of the batteries is not investigated in the total cost of the scheme. Similarly, in [15], a linear layout for co-optimization operation and planning of PEVs, SWSs, and different types of DERs was

presented based on V2G and vehicle-to-SW (V2S) concepts, considering the uncertainties of DERs and PEVs. The authors of [16] proposed an optimization problem to minimize the entire cost of the energy and apply RBE to achieve optimum operation in SCs. The proposed model is linear and the uncertain behavior of transportation systems and loads is depicted. A management framework utilizing V2G and V2S is proposed in [17] to attain the maximum performance of the transportation systems. Additionally, blockchain technology has been employed to enhance the security of exchanged information in the SC.

In [18], the authors propose the multi-swarm differential evolutionary particle swarm optimization algorithm to optimize a mixed-integer nonlinear programming problem for energy management in an SC. However, the interconnection between different parts of the SC model is not covered thoroughly.

In previous studies, the nonlinear effects of the network model, the consideration of depth of discharge (DoD) for a more realistic battery model, as well as the effects of the subway, electric vehicle (EV), and DER have not been investigated simultaneously, and issues such as the effect of EVs entering the network have only been investigated separately. Therefore, in this paper, for the first time, to show the network model more realistically, nonlinear effects have been considered in the system model, and also to be closer to the real battery model, the DOD of the battery has been considered. In addition, in the proposed SC model, EVs and subways, as well as different types of DER, have been discussed simultaneously. Also, in this article, real models of PV, HP, and EV have been used to obtain a real model of an SC.

Two main methods exist for solving optimization problems similar to the problem in this research. The first one is using exact algorithms that can provide an exact global optimum. However, the execution time of the exact algorithms is raised exponentially in proportion to the number of variables [19]. In contrast, approximate optimization algorithms can find optimal/near-optimal solutions in a reasonable amount of time [20]. The grey wolf optimization algorithm (GWOA) is a nature-inspired optimization algorithm. GWOA has been widely used due to its simplicity, fewer control variables, and easy implementation [20]. However, GWOA has some deficiencies that researchers have attempted to overcome in the i-GWOA provided in [20]. Further explanations are provided in Section 3 of this paper.

The objective of this paper is the optimal planning and operation of the SC model considering synergies between SWSs and PEVs in the presence of different DER technologies. Multiple scenarios are considered to assess the proposed layout. Additionally, the destruction cost of the batteries is calculated and added to the total cost. This adds some nonlinear terms to the problem, and, as a result, an intelligent algorithm must be utilized to solve the problem. To solve this optimization problem, the i-GWOA was utilized and was observed to be fully capable of solving the optimization problem in this study.

The main contributions of this study are presented as follows:

- A comprehensive SC layout considering PEVs, metro system, DER technologies, and the interconnection between them is presented.
- The total cost of the SC model is improved by utilizing the i-GWOA that is illustrated through different case studies and scenarios.
- Various DER technologies, such as PV, HP, and batteries are incorporated into the model and their impact is analyzed.
- The destruction cost of batteries is considered along with losses regarding PVs and HPs to achieve a more realistic and comprehensive model.
- Different kinds of algorithms such as GA, PSO, DE, BBO-DE, and GWOA are compared to find the best and fastest way to solve the SC problem.

The remainder of the paper is organized as follows. Section 2 describes the mathematical formulation of the problem. Section 3 presents the solution of the i-GWOA. The proposed SC model and case study descriptions are provided in Section 4. The simulation outcomes and discussion are presented in Section 5. Finally, the conclusions and future horizons of the work are presented in Section 6.

2. Problem Formulation

2.1. Planning

Here, a detailed description of the mathematical formulation of the linear optimization problem is presented. The objective function (OF) of the problem has been proposed in Equation (1):

$$\min\left(\text{cost}_{h}^{E}+\text{cost}_{h}^{P}+\text{cost}^{Eth}+\text{cost}^{Pth}+\text{cost}_{inv\&om}^{PV}+\text{cost}_{inv\&om}^{HP}+\text{cost}_{inv}^{Bat}+\text{cost}_{eq}^{DR}+\text{cost}_{sub}^{E}+\text{cost}_{sub}^{P}+\text{cost}^{EV}\right) \quad (1)$$

Equations (2)–(14) are used to define the different terms in Equation (1). In Equations (2) and (3), the costs of power and electric energy for the housing area are presented, respectively.

$$\text{cost}_{h}^{E}=\sum_{y}\left(\text{ECost}_{y}^{inc}*\sum_{m.h}\left(\text{Day}_{m}*\left(\text{EBuy}_{m.h}^{res}*\text{P}_{m,h}^{BuyGrid}-\text{ESell}_{m,h}*\text{P}_{m,h}^{SellGrid}\right)\right)\right) \quad (2)$$

$$\text{cost}_{h}^{P}=\sum_{y}\left(\text{ECost}_{y}^{inc}*\text{Tariff}^{E}*\text{P}^{EContract}\right) \quad (3)$$

The cost of electric energy is calculated using the base residential price of electricity, the base selling price of electricity, and the annual growth in the base purchase price of electricity. The power cost presented in Equation (3) is calculated using the annual tariff for residential power and the annual growth in the purchase price of electricity multiplied by the annual contracted power.

Equations (4) and (5) denote the thermal energy and thermal power costs of the area. TCost_{y}^{inc} represents the annual growth of the purchase price of thermal energy, and Tariff^{T} represents the annual tariff for residential thermal power:

$$\text{cost}^{ETh}=\sum_{y}\left(\text{TCost}_{y}^{inc}*\sum_{q,m}\left(\text{Day}_{m}*\text{P}_{q,m}^{ThBuy}\right)\right) \quad (4)$$

$$\text{cost}^{Pth}=4*\text{n}_{span}*\text{n}_{house}*\text{Tariff}^{T} \quad (5)$$

Equation (6) corresponds to the investment, operation, and maintenance costs of the PV. Equation (7) represents the investment, operation, and maintenance costs of HP. In Equation (8), the battery investment costs in the proposed method are represented, and Equation (9) presents the cost related to the equipment that is needed for each customer to perform load shifting.

$$\text{cost}_{inv\&OM}^{PV}=\sum_{q}\left(\text{Cost}_{ins}^{PV}*\text{Cap}_{q}^{PV}\right)+\left(\text{OM}_{annual}^{PV}*\text{Cap}_{q}^{PV}*\text{n}_{span}\right) \quad (6)$$

$$\text{cost}_{inv\&OM}^{HP}=\sum_{q}\left(\text{Cost}_{ins}^{HP}*\text{Cap}_{q}^{HP}\right)+\left(\text{OM}_{annual}^{HP}*\text{Cap}_{q}^{HP}*\text{n}_{span}\right) \quad (7)$$

$$\text{cost}_{inv}^{Bat}=\sum_{q}\left(\text{cost}_{ins}^{Bat}*\text{Cap}_{q}^{Bat}\right) \quad (8)$$

$$\text{cost}_{eq}^{DR}=4*\text{n}_{house}*\text{cost}_{eq}^{ls} \quad (9)$$

The demand response is considered as the ability to shift loads in a residential area and has been set to a maximum of 13% of the total load in a typical house. Additionally, it has been supposed that the residential region does not have any type of DER installed beforehand [21].

In Equation (10), the upfront cost of the PEV batteries at the beginning of the 20-year study period was calculated. Cost_{ins}^{Bat} represents the upfront cost of the stationary batteries. Finally, the equations that formulate the cost of SW power and SW energy are presented in

Equations (11) and (12). $\text{Tariff}_{\text{sub}}$ represents the annual tariff for SW power during different usage profiles. $D^{\text{sub}}_{\text{m,h}}$ represents the SW consumption curve after changing the profile:

$$\text{cost}^{\text{EV}}_{\text{inv}} = (\text{cost}^{\text{Bat}}_{\text{ins}} * n_{\text{EV}} * C_{\text{EV}}) \tag{10}$$

$$\text{cost}^{\text{P}}_{\text{sub}} = \sum_{\text{y}} \text{ECost}^{\text{inc}}_{\text{y}} * \left(\left(\text{Tariff}^{\text{peak}}_{\text{sub}} * P^{\text{peak}}_{\text{sub}}\right) + \left(\text{Tariff}^{\text{mid}}_{\text{sub}} * P^{\text{mid}}_{\text{sub}}\right) + \left(\text{Tariff}^{\text{off}}_{\text{sub}} * P^{\text{off}}_{\text{sub}}\right)\right) \tag{11}$$

$$\text{cost}^{E}_{\text{sub}} = \sum_{y} \left(\text{ECost}^{\text{inc}}_{y} * \sum_{\text{m,h}} \left(\text{Day}_{m} * \text{EBuy}^{\text{res}}_{\text{m,h}} * D^{\text{sub}}_{\text{m,h}}\right)\right) \tag{12}$$

It is considered that all investments were made at the beginning of the study period (20 years). The stationary batteries of the clients are assumed to be replaced every eight years [22]. PEV batteries are also supposed to be replaced every five to eight years because of the additional destruction caused by coupling usage with the SW [23].

Equation (13) is the electrical energy balance equation that ensures the balance between all the electrical energy that enters and all the electrical energy that exits each node of the system. $D^{new}_{q,m,h}$ is the consumption curve after changing the profile, and $\eta^{EV}_{D}/\eta^{EV}_{C}$ are the discharge/charge efficiencies of the PEV batteries. In Equation (14), all the energy that is entering is separated from all the energy that is leaving to address the sold and bought energy more efficiently. In Equation (15), the thermal energy is balanced, similar to the electrical energy using the total thermal demand ($D^{New}_{q,m,h}$), energy saving owing to efficiency measures (η_{energy}), and the total loss of the HP system ($loss^{HP}$). Several loss sources exist in HPs, including throttling losses, superheating, pressure drop, compressor efficiency, temperature driving forces, and mismatch amongst process and HP fluids [24,25]. Here, the HP loss is assumed to be equal to 15 percent of the total power, as presented in Table 1. In addition, C_{HP} represents the coefficient of performance related to the HP system.

$$\text{E}^{\text{Grid}}_{\text{m,h}} = \sum_{\text{q}} \left(\text{D}^{\text{new}}_{\text{q,m,h}} - \text{P}^{\text{PV}}_{\text{q,m,h}} - \left(\text{P}^{\text{BatDis}}_{\text{q,m,h}} * \eta^{\text{EV}}_{\text{D}}\right) + \left(\text{P}^{\text{BatCh}}_{\text{q,m,h}}/\eta^{\text{EV}}_{\text{C}}\right) + \text{P}^{\text{inHP}}_{\text{q,m,h}}\right) + \sum_{\text{y}} \left(\left(\text{P}^{\text{EV,ch}}_{\text{v,m,h}}/\eta^{\text{EV}}_{\text{C}}\right) - \left(\text{P}^{\text{EV,dch}}_{\text{v,m,h}}/\eta^{\text{EV}}_{\text{D}}\right)\right) \tag{13}$$

$$\text{E}^{\text{Grid}}_{\text{m,h}} = \text{P}^{\text{BuyGrid}}_{\text{m,h}} - \text{P}^{\text{SellGrid}}_{\text{m,h}} \tag{14}$$

$$\text{P}^{\text{ThBuy}}_{\text{m}} = \sum_{\text{q}} \left(\left(\text{D}^{\text{Th}}_{\text{q,m}} * \left(1 - \eta_{\text{energy}}\right) * 0.8\right) - \sum_{\text{h}} \left(\text{P}^{\text{inHP}}_{\text{q,m,h}} * \left(1 - \text{loss}^{\text{HP}}\right) * \text{C}_{\text{HP}}\right)\right) \tag{15}$$

Table 1. Second scenario of the fleet characteristics.

Fleet Number	Number of PEV	Access Time (h) in		Capacity (KWh)		Charge/Discharge Rate (KWh)	
		Grid Parking	Subway Parking	Min	Max	Min	Max
1	68	1–7, 16–24	6–18	263	1973	7.3	496
2	40	1–7, 16–24	6–18	219	1644	7.3	292

The mathematical model for PEVs is formulated in Equations (16)–(22). Equation (16) ensures that the initial SOC of the PEVs in the first hour of each month is equal to that in the last hour of the previous month. Furthermore, it is shown in Equation (17) that the initial and final SOCs of PEVs are assumed to be the same for each month. As shown in Equation (18), the SOC of PEVs is restricted based on the minimum SOC required for EVs to arrive at the parking lot and different types of PEV users.

$$\text{SOC}^{\text{EV}}_{\text{v,m,h=0}} = \text{SOC}^{\text{EV}}_{\text{v,m-1,h=24}} \text{ for } 2 \le \text{m} \le 12 \tag{16}$$

$$\text{SOC}^{\text{initialEV}}_{\text{v,m}} = \text{SOC}^{\text{finalEV}}_{\text{v,m}} \text{ for } 2 \le \text{m} \le 11 \tag{17}$$

$$\mathrm{SOC}_{v,h}^{\mathrm{minEV}} * n_{EV} \leq \mathrm{SOC}_{v,m,h}^{EV} \leq \mathrm{Cap}_{v,h}^{\mathrm{MaxEV}} * n_{EV} \quad (18)$$

The SOC is calculated using Equation (19) using the SOC for the previous hour, the amount of electricity charged/discharged into/from the PEV battery, and the amount of electricity traded (charged/discharged) with the SWS. Equation (20) is used to ensure that the amount of electricity discharged from the PEV is less than its SOC in the previous hour. The binary variables $U_{v,m,h}^{EV}$ in Equation (21) indicate the presence of PEVs at the charging station. If $U_{v,m,h}^{EV}$ equals 1, the PEV is plugged into and exchanges power with the grid and is being charged or discharged. Conversely, if $U_{v,m,h}^{EV}$ equals zero, the PEV is not plugged in and does not exchange power with the grid. Finally, Equations (22) and (23) indicate the limits for the discharge and charge of the PEV batteries.

$$\mathrm{SOC}_{v,m,h}^{EV} = \mathrm{SOC}_{v,m-1}^{EV} - \left(P_{v,m,h}^{EVdis} * \eta_D^{EV}\right) + \left(P_{v,m,h}^{EVch} * \eta_C^{EV}\right) + \left(\mathrm{SOC}_{v,h}^{arrive} * \eta_{EV}\right) - \left(P_{v,m,h}^{Sub,dis} * \eta_D^{sub}\right) + \left(P_{v,m,h}^{Sub,ch} * \eta_C^{Sub}\right) \quad (19)$$

$$P_{v,m,h}^{EVdis} \leq \mathrm{SOC}_{v,m,h-1}^{EV} \quad (20)$$

$$U_{v,m,h}^{EVdis} + U_{v,m,h}^{EVch} = U_{v,m,h}^{EV} \quad (21)$$

$$U_{v,m,h}^{EVdis} \underline{P_{v,m,h}^{EVdis}} \leq P_{v,m,h}^{EVdis} \leq \overline{P_{v,m,h}^{EVdis}} U_{v,m,h}^{EVdis} \quad (22)$$

$$U_{v,m,h}^{EVch} \underline{P_{v,m,h}^{EVch}} \leq P_{v,m,h}^{EVch} \leq \overline{P_{v,m,h}^{EVch}} U_{v,m,h}^{EVch} \quad (23)$$

The SWS is modeled using Equations (24)–(30). Equation (24) indicates that the amount of energy charged into the PEV batteries is limited to the SW regenerative BE. In Equation (25), the power discharged from the SWS is guaranteed to be lower than the SOC of the SW battery in the previous hour. The new SW consumption curve is calculated by Equation (26). Equation (27) ensures that the contracted power for the SWS is higher than the new consumption curve for all tariff intervals (off-peak, peak, and mid-peak). The binary variable $U_{v,m,h}^{Sub}$ in Equation (28) indicates the connection of the PEVs with the SWS. If $U_{v,m,h}^{Sub}$ equals 1, the PEV is connected to the SWS, exchanges power with the SW, and is charged or discharged. Conversely, if $U_{v,m,h}^{EV}$ equals zero, the PEV is not connected to the SWS and does not exchange power with the SW. The limits for the discharge and charge of the SWS are presented in Equations (29) and (30), respectively.

$$\sum_{v} P_{v,m,h}^{Subch} \leq RB_h^{Sub} \quad (24)$$

$$P_{v,m,h}^{Subdis} \leq \mathrm{SOC}_{v,m,h-1}^{Sub} \quad (25)$$

$$D_{m,h}^{Subnew} = RB_h^{Sub} - \sum_{v} P_{v,m,h}^{Subdis} \quad (26)$$

$$\begin{cases} P_{Sub}^{off} \geq D_{off}^{Subnew} \\ P_{Sub}^{mid} \geq D_{mid}^{Subnew} \\ P_{Sub}^{peak} \geq D_{peak}^{Subnew} \end{cases} \quad (27)$$

$$U_{v,m,h}^{Subdis} + U_{v,m,h}^{Subch} = U_{v,m,h}^{Sub} \quad (28)$$

$$U_{v,m,h}^{Subdis} \underline{P_{v,m,h}^{Subdis}} \leq P_{v,m,h}^{Subdis} \leq \overline{P_{v,m,h}^{Subdis}} U_{v,m,h}^{Subdis} \quad (29)$$

$$U_{v,m,h}^{Subch} \underline{P_{v,m,h}^{Subch}} \leq P_{v,m,h}^{Subch} \leq \overline{P_{v,m,h}^{Subch}} U_{v,m,h}^{Subch} \quad (30)$$

Equation (31) indicates that the power drained by the HP is limited by its installed capacity. The HP operation is modeled by Equation (32), where its output should follow a specified thermal demand.

$$P_{q,m,h}^{inHP} \leq \mathrm{Cap}_q^{HP} \quad (31)$$

$$\sum_{h} P_{q,m,h}^{inHP} * \left(1 - loss^{HP}\right) * C_{HP} \geq (1 - \eta_{en}) * D_{q,m}^{Th} * 0.8 * D_{h}^{nTh} \quad (32)$$

PVs are widely used in smart cities to decrease CO_2 pollution by producing clean electricity:

$$P_{q,m,h}^{PV} = Cap_{q}^{PV} * \frac{\Omega_{m,h}}{\Omega_{TC}} * (1+K_T(T_c - T_a)) * (1 - loss^{PV}) \quad (33)$$

The power produced by the PV is modeled in Equation (33). $\Omega_{m,h}$ is the global horizontal irradiation at the current location (W/m^2). Ω_{TC} is the global horizontal irradiation at the test condition. T_c is the temperature of the PV cell. T_a is the temperature of the atmosphere [12]. The PV loss can be caused by various environmental and operational factors. These factors include dust allocation, soiling effect, and humidity [26]. Here, for the sake of simplicity, the PV loss is assumed to be equal to 24 percent, as stated in Table 2.

Table 2. DER costs and expected energy losses.

Technology	Installation Cost	OM Cost	Losses (%)
PV	2.15 (EUR/W)	30.93 (EUR/KW)	24 (electric)
HP (C_{HP} = 2.5)	2.94 (EUR/W)	100.1 (EUR/KW)	15 (thermal)
Battery	0.36 (EUR/W)	-	10 (electric)

2.2. Operation

PEVs can charge or discharge by connecting to the grid and SWS when arriving at a parking lot daily. The PEV cost must be added to the OF to optimize the operation of the PEVs.

The PEV cost includes two terms when the daily operation of the PEVs is considered, as shown in Equation (34). The first expression defines the cost of PEV power, which is according to the number of PEVs and the amount of power being charged or discharged. Equation (35) presents the formulation for the PEV operational cost. The subsequent expression defines the destruction cost of PEV batteries.

$$Cost_{op}^{EV} = Cost_{pow}^{EV} + Cost_{deg}^{EV} \quad (34)$$

$$Cost_{pow}^{EV} = \sum_{h,n_{EV}} C_h * P_h^{EV} \quad (35)$$

The destruction cost of the battery is a consequence of the charging/discharging cycles of the battery. According to [27], the number of cycles for which a battery can be charged and discharged depends on the DoD through the Wöhler curve. An example of a Wöhler curve for a typical battery is shown in Figure 1. It has been seen that the number of cycles in the battery lifespan increases as DoD increases. Equation (36) presents the mathematical formulation of the Wöhler curve. a and b express constants related to the kind of battery and $n_{cycle}(DoD)$ is the number of possible cycles based on the amount of DoD [27]. For a Li-ion battery manufactured by Saft company, the parameters $a = 1331$ and $b = -1.825$ are obtained [28].

The destruction cost for discharging a battery from a fully charged status—that is, a DoD equal to zero—to a specific level—that is, a DoD equal to DoD_{spec}—is calculated in Equation (37). E^{EVBat} is the battery's usable energy in kWh.

$$n_{cycle}(DoD) = a.DoD^{b} \quad (36)$$

$$Cost_{deg}(0, DoD_{spec}) = \frac{Cost_{inv}^{EVBat} * DoD_{spec} * E^{EVBat}}{n_{cycle}(DoD_{spec})} \quad (37)$$

The destruction cost of a discharge cycle from $DoD_{initial}$ to DoD_{final} was calculated using Equation (38). Finally, Equation (39) presents the entire destruction cost, which is the sum of destruction costs over the number of discharges.

$$Cost_{deg}(DoD_{initial}, DoD_{final}) = Cost_{deg}(0,DoD_{final}) - Cost_{deg}(0, DoD_{final}) \quad (38)$$

$$Cost_{deg}^{EV} = \sum_{n_{dis}} Cost_{deg,n}(DoD_{initial}, DoD_{final}) \quad (39)$$

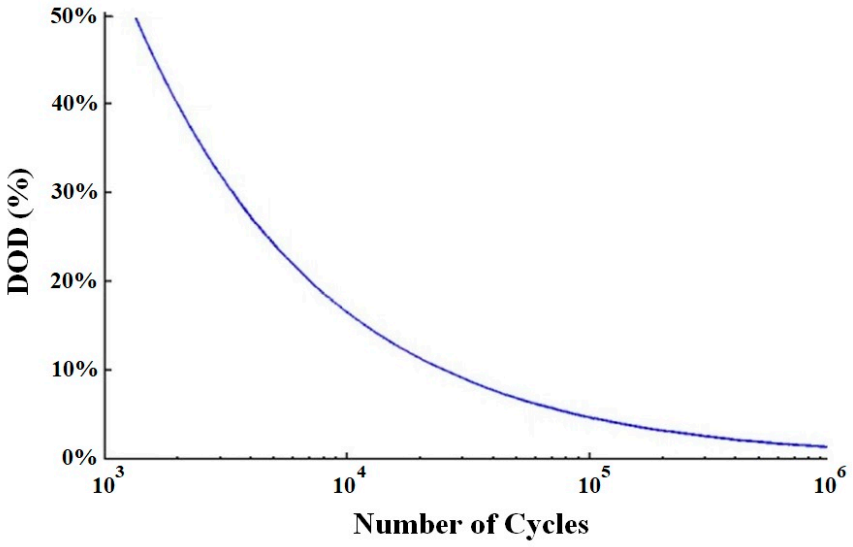

Figure 1. Wöhler curve for lithium-ion battery.

3. Solution Algorithm

3.1. Algorithm Description

This section provides a solution to the optimization problem formulated in the previous section.

The solution method was based on the i-GWOA. The GWOA is a metaheuristic optimization algorithm on the basis of the hunting activities of gray wolves in nature. In the GWOA, three wolves named α, β, and γ are the best solutions in each iteration and are chosen to lead the remaining wolves to find the global optimum solution [20]. GWOA is presented in Equations (40)–(47): Equations (40)–(44) model the "encircling" process, where W_i is the situation of a wolf and X_i^p is the situation of the prey in the i-th iteration. In addition, $rand_1$ and $rand_2$ are random vectors in the range of [0, 1].

$$C_1 = \left|C_2 \times X_i^p - W_i\right| \quad (40)$$

$$W_{i+1} = X_i^p - C_3 \times C_1 \quad (41)$$

$$C_3 = 2 \times C_3 \times rand_1 - A_i \quad (42)$$

$$C_2 = 2 \times rand_2 \quad (43)$$

$$A_i = 2 - (2 * i)/i_{max} \quad (44)$$

In this stage, all wolves are restricted to follow the three best solutions (α, β, and γ). This "hunting" behavior of the wolves is modeled by Equations (45)–(47), where $C_2(1)$, $C_2(2)$, and $C_2(3)$ are calculated using Equation (43). N_w is the wolf population number.

$$C_1^\alpha = |C_2(1) \times W^\alpha - W_i| C_1^\beta = \left|C_2(2) \times W^\beta - W_i\right| C_1^\gamma = |C_2(3) \times W^\gamma - W_i| \quad (45)$$

$$W_i^n(1) = W_i^\alpha - C_3^n(1) \times C_{1,i}^\alpha W_i^n(2) = W_i^\beta - C_3^n(2) \times C_{1,i}^\beta W_i^n(3) = W_i^\gamma - C_3^n(3) \times C_{1,i}^\gamma; \forall n \in [1, N_w] \quad (46)$$

$$W_{i+1}^{n\text{-}GW} = \frac{W_i^n(1) + W_i^n(2) + W_i^n(3)}{3};\ \forall n \in [1, N_w] \tag{47}$$

In the i-GWOA implemented here, a few steps are added to overcome the issues of the GWOA. These issues include obtaining locally optimum solutions by relying on the three best solutions only and the low diversity of the population [20]. These additional steps provide a different search strategy based on the neighbors surrounding each wolf.

Equation (48) calculates the radius by using the distance amongst the current situation of the n-th wolf and the calculated situation in Equation (47). Then, Equation (49) is used to build the set of neighbors, where D^n is the distance between n-th and m-th wolves. Furthermore, the d-th dimension of the answer for the new search strategy is calculated in Equation (50) using the d-th dimension of a random wolf from the neighbors ($W_i^{b,d}$), and the d-th dimension of a random wolf from the population ($W_i^{r,d}$).

$$R_i^n = \left| |W_i^n - W_{i+1}^{n\text{-}GW}| \right| \tag{48}$$

$$N_i^n = \left\{ W_i^m \middle| D^n\left(W_i^n, W_i^M\right) \le R_i^n, W_i^m \in pop \right\} \tag{49}$$

$$W_{i+1}^{n\text{-}iGW,d} = W_i^{n,d} + rand \times \left(W_i^{b,d} - W_i^{r,d}\right) \tag{50}$$

Finally, Equation (51) is used to select the best answer by comparing the fitness amounts of the different search strategy answers. The pseudocode and diagram for the i-GWOA have been depicted in Algorithm 1 and Figure 2.

$$W_{i+1}^n = \begin{cases} W_{i+1}^{n\text{-}GW} \text{ if } f\left(W^{n\text{-}GW}\right) \le f\left(W^{n\text{-}iGW}\right) \\ W_{i+1}^{n\text{-}iGW} \quad \text{O.W} \end{cases} \tag{51}$$

Algorithm 1: The pseudocode of i-GWOA.

Set N_w The number of wolves
Set D The number of dimensions
Set i_{max} Maximum iteration number
Input: D, N_w, i_{max}
Output: The global optimum
Begin
  Initialize: Distribute N_w wolves randomly and generate an initial population that satisfies the constraints
  Release Entire of the constraints of the problem via using Equation (53)
  For i = 1 to i_{max}
    Find W^{α}, W^{β}, and W^{γ}
    For n = 1 to N_w
      Calculate $W_i^n(1)$, $W_i^n(2)$, $W_i^n(3)$, using Equation (46)
      Calculate W_{i+1}^{n-GW}, using Equation (47)
      Calculate R_i^n, using Equation (48)
      Construct N_i^n within R_i^n radius, using Equation (49)
      For d = 1 to D
        Calculate W_{i+1}^{n-iGW}, using Equation (50)
      End
    Select the best answer
    Update population
    End
  End

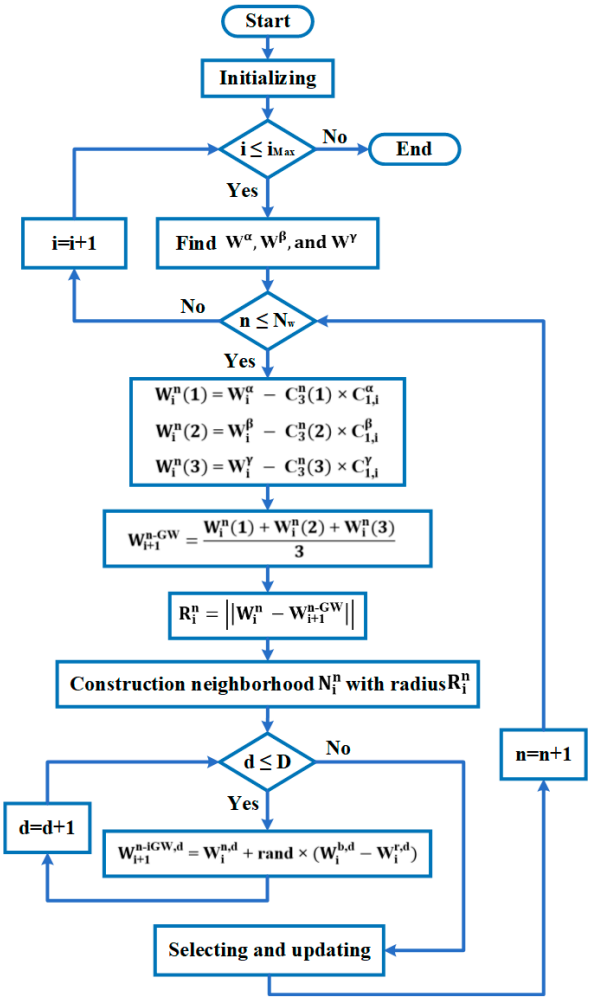

Figure 2. The diagram of the i-GWOA.

3.2. Implementing the i-GWOA for the Proposed Problem

In this section, the implementation of the i-GWOA on the SC problem is presented step by step to clarify the solution process.

- Step 1: Set input values including the number of parameters, the population, and maximum iterations. Here, the population number is considered to be 400, and the maximum number of iterations is set to 700;
- Step 2: Produce the primary population randomly. In addition, the initial population must satisfy the inequality and equality constraints. In order to ensure this, vectors X_{min} and X_{max} are calculated according to the minimum and maximum bounds of the parameters. Then, the initial population is calculated using the following equation, where rand is a random vector between [0, 1];

$$\bar{X}_{pop} = (rand * (X_{max} - X_{min})) + X_{min} \quad (52)$$

This process is repeated for every variable for the population number, so that the initial population is calculated.

- Step 3: Release the entire constraints of the problem by using the below equation:

$$G(X) = \left[f\left(\bar{X}\right) \right] + L_1 \left(\sum_{1}^{N_{eq}} (h_{eq}(\bar{X}))^2 \right) + L_2 \left(\sum_{1}^{N_{ineq}} (Max \left[0, -g_{ineq}(\bar{X}) \right])^2 \right) \quad (53)$$

where $f(\overline{X})$ is the OF of the problem. $h_{eq}(\overline{X})$ and $g_{ineq}(\overline{X})$ define the equality and inequality constraints, respectively. Here, two parameters that affect the performance of the algorithm are L_1 and L_2 penalty amounts. If the selected penalty amounts are too high, the algorithm can become trapped in local minima. Conversely, if the selected penalty amounts are too low, they cannot diagnose feasible optimum solutions. Here, an adaptive penalty function used in [18] is adopted to handle penalty factors. For the sake of brevity, $\sum_1^{N_{eq}} (h_{eq}(\overline{X}))^2$ and $\sum_1^{N_{ineq}} (\text{Max } [0, -g_{ineq}(\overline{X})])^2$ are expressed as B and $L_1 = L_2 = i\sqrt{i}\lambda B^{\delta}$. Here, i is the iteration number, λ defines a multi-stage assignment amount, and δ defines the power of the penalty amount. Here, if $B \leq 1$ then $\delta = 1$; otherwise, $\delta = 2$. Moreover, if $B \leq 0.001$, then $\lambda = 1$, or if $B \leq 0.01$, then $\lambda = 10$, or if $B \leq 0.1$, then $\lambda = 30$; otherwise, $\lambda = 100$.

- Step 4: Calculate the OF with the population. Sort the population according to the OF amounts. Then, set the three best individuals as α, β, and γ;
- Step 5: Calculate W_{i+1}^{n-GW} using Equations (46)–(49);
- Step 6: Calculate W_{i+1}^{n-iGW} using Equation (50);
- Step 7: Select and update each individual of the population based on Equation (53);
- Step 8: Check the maximum iteration number. If it is not reached, go to step 4, and continue until the maximum iteration number is reached.

4. SC Model and Case Studies

4.1. SC Model and Parameters

The presented model of the SC consists of an electric substation associated with the SWS and PEV parking that is connected to the electric substation for energy transactions between them, and a residential area that contains loads, and is augmented with certain DER technologies, including PVs, HPs, and batteries. All these segments are coupled with the grid. It is notable that the connection amongst the PEVs and the SWS consists of the railway power line, an ESS, and the charging posts for the PEVs. These parts are connected through DC links [14]. An illustration of the suggested layout is shown in Figure 3.

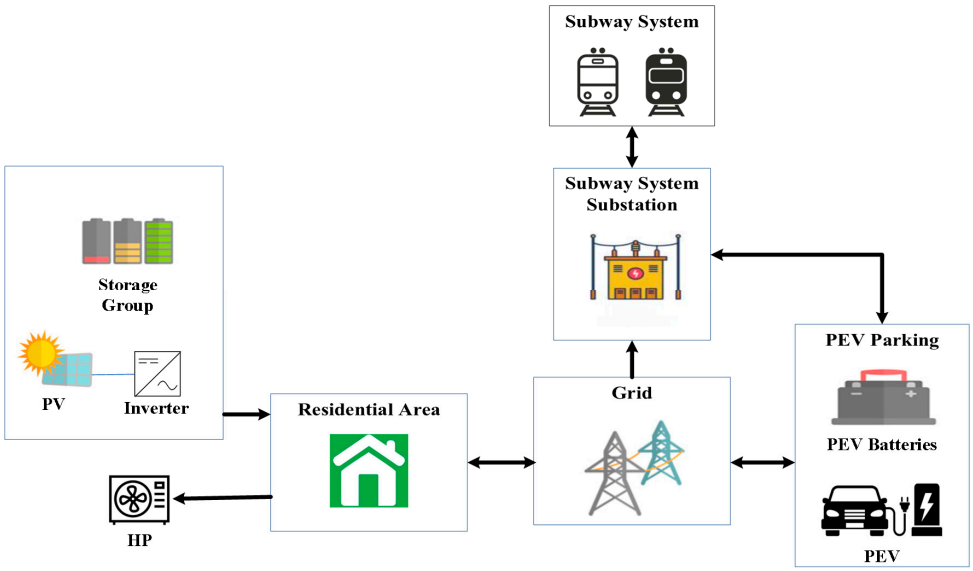

Figure 3. Illustration of the SC model.

To model the electric substation, it is assumed that 80 percent of the total energy consumed by the SWS is relevant to the trains' traction energy, and only 33 percent of this energy can be retrieved through regenerative braking [29,30]. Figure 4 illustrates the energy profile of the SW substation obtained from [30].

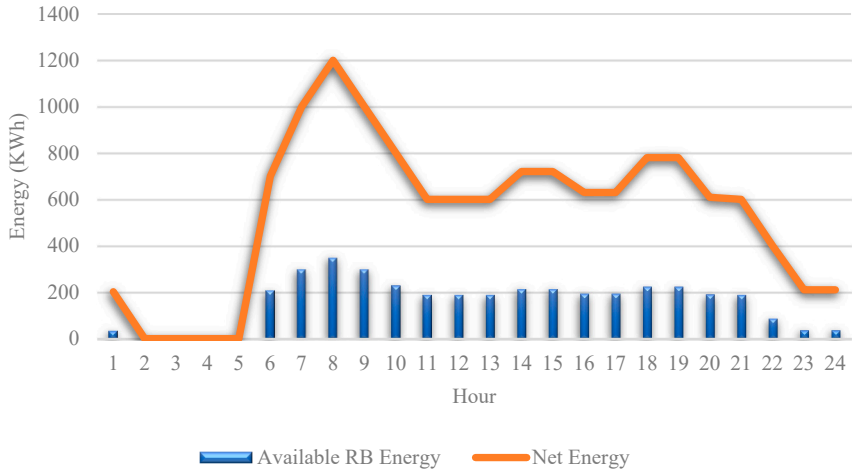

Figure 4. Substation energy profile.

Two different scenarios are proposed for PEVs. In the first one, taken from [14], a parking lot with 194 spots and two different types of PEV users (local and traveler) is considered. Local users utilize parking at night when they arrive at their homes, whereas travelers who come to the neighborhood use parking during the day when the locals have left. To extend the battery life, it is assumed that the minimum SOC of the parked PEVs is 20 percent and the maximum SOC when the PEV leaves is 80 percent [31].

In addition, the storage capacity of each PEV was 19 kWh [32]. The energy required for the trip is considered to be 40 percent of the maximum capacity, meaning that the PEV enters the parking space with an SOC of 40 percent. The time-of-use and minimum SOC requirements of the PEV users are shown in Figure 5.

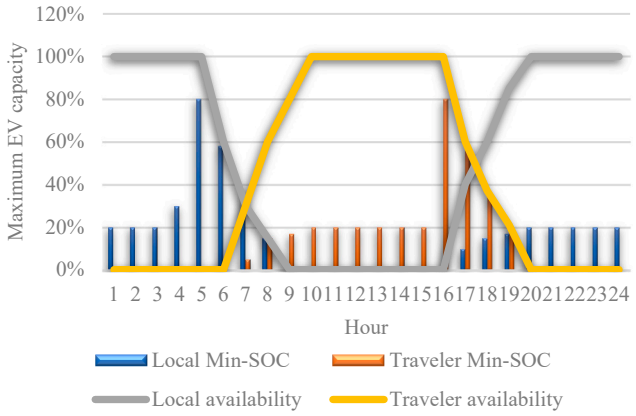

Figure 5. PEV users' time-of-use and minimum SOC requirements.

The second scenario considers two PEV fleets with different characteristics, as presented in Table 1. Each fleet consists of several PEVs that take two trips throughout the day. It is considered that the SOC of the PEV fleets is 100 percent when they leave the parking lot for the initial trip.

The PEV batteries are assumed to be typical lithium-ion batteries. The Wöhler curve parameters (a and b) for this battery type were 1331 and −1.825 respectively. The battery investment cost was assumed to be EUR 300.

The solar production of the PV is computed using mean solar global horizontal irradiance data for Madrid, at 35° inclination and facing south [33]. The PV panels that are used here are mono-crystalline silicon, the same parameters described in [34].

The costs and parameters of the different DERs studied here are presented in Table 2. Figure 5 shows the daily solar radiation profile during summer [15]. Moreover, a maximum

of thirteen percent of the daily load is allowed to be shifted [21], and the cost of tools needed for performing load shifting is assumed to be EUR 250/house [35].

The considered residential area was assumed to contain 250 houses with different user types and different energy usage patterns [36]. The residential electricity usage was modeled by a time-of-use electricity tariff presented in Table 3 [37,38]. In addition, the thermal energy tariff was considered to be constant. SW time-of-use energy and power tariff values are shown in Table 4, which also includes different time schedules during the winter and summer months.

Table 3. Residential energy tariffs.

	Peak	Mid-Peak	Off-Peak
Electric Energy (EUR/kWh)	0.1632	0.0843	0.0564
Electric Power (EUR/kW)	-	49.2862	-
Time schedule	13–23 h	7–13, 23–1 h	1–7 h
Natural gas variable (EUR/kWh)		0.0567	
Natural gas fixed (EUR/year)		0.05232	

Table 4. SW energy tariffs.

	Peak	Mid-Peak	Off-Peak
Electric Energy (EUR/kWh)	0.1266	0.1092	0.0804
Electric Power (EUR/kW)	59.4753	36.6768	8.4104
Winter schedule	17–23 h	8–17, 23 h	0–8 h
Summer schedule	10–16 h	8–10,16–0 h	0–8 h

4.2. Case Studies

Four different case studies are presented in this paper to thoroughly demonstrate the impact of interconnections between PEVs and SWSs, along with the impacts of implementing different DER technologies in the model. A base case (C^{Base}) was presented as a benchmark for evaluation and comparison with other case studies. In this case, there is no interconnection between the PEVs and the SWS, and no DER technologies are present.

The second case study (C^{Con}) assesses the interconnection between PEVs and the SWS without considering DER technologies. In the third case study (C^{DER}), DER technologies were considered, but the PEVs and SWS were optimized separately. Finally, in the fourth case study ($C^{Con+DER}$), both DER technologies and the connection between PEVs and SWSs were considered.

5. Simulation Results

5.1. Case Study Results

In this section, the simulation outcomes for each scenario have been provided and compared with each other. The layout has been carried out in a MATLAB 2019a simulation environment, and the simulations were performed on a standard laptop with a Core i7 processor and 8 gigabytes of RAM. The runtime for each simulation is approximately 60 s.

The total cost for each case study, based on the first PEV scenario, is shown in Figure 6. It can be observed that for C^{Base}, the total cost is EUR 37.2 million when 25 PEVs are considered. The total cost gradually increases when the number of PEVs increases. This growth was caused by the increase in PEV loads, as the other costs remained the same. In addition, the SWS remains the same because no interconnection is considered. In the next case study of C^{Con}, the interconnection between the PEVs and SWS is considered.

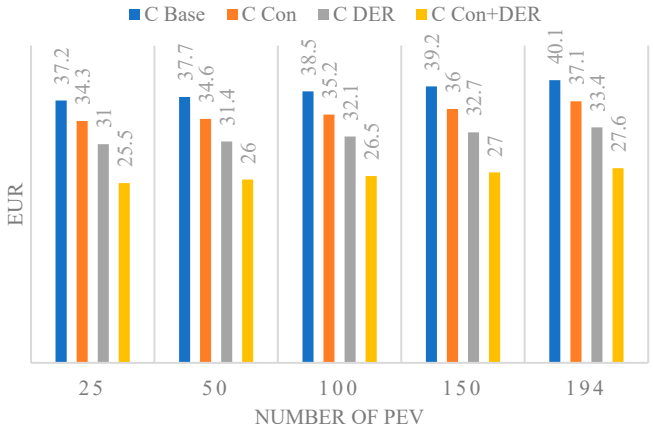

Figure 6. Total cost of each case study for different PEV numbers in the first PEV scenario.

It can be seen that the entire cost for this case study was lower than that of the base case. This is caused by a decrease in SWS costs because of the interconnection, and the SWS being able to take advantage of the higher storage capacity provided by PEVs.

For C^{DER}, although the SW costs are the same as in the base case, and the investment costs are higher, it can be noted that the entire cost is lower than in the previous cases. This occurred as a consequence of electrical and thermal generation of PV and HP, respectively, resulting in less energy being bought from the grid, in addition to load shifting being considered. Finally, in the final case study ($C^{Con+DER}$), where both the interconnection and presence of DER technologies are considered, the total cost shows a significant decrease.

Figure 7 illustrates the operation of the PEVs and DER technologies on a typical summer day considering $C^{Con+DER}$. It can be observed that the PEVs and stationary battery charge when the solar radiation and PV power production are high, and discharge when solar radiation and PV power production are low, in that they supply other loads in the SC model. As shown in Table 2, the investment costs of stationary batteries are significantly lower than those of PVs. This has resulted in the battery capacity being higher than the installed PV capacity, resulting in a system that exploits the high battery capacity and reduces overall costs. The optimal operation of different parts of the model caused a decrease that has been observed in the total cost rate.

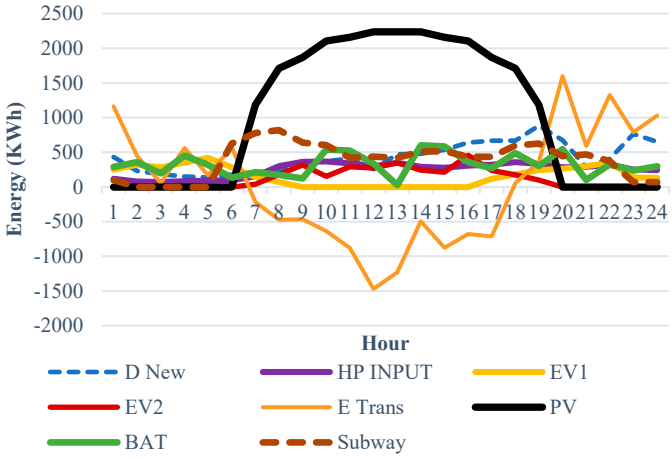

Figure 7. Daily operation of DER, PEV, and the SWS in summer for the first scenario.

A percentage-based comparison of the different costs of the case studies is presented in Table 5. It can be seen that in C^{DER}, no change in SW costs is observed, but a rather large decrease in residential area costs has occurred. The residential area costs decreased by up to 53.6% compared to the base case. In addition, the thermal costs were reduced significantly by up to 95 percent owing to the thermal energy generation of the HP system. The total

cost decreased by approximately 16.6 percent in this case study. On the other hand, C^{Con} resulted in a 35.7 to 50 percent decrease in SW costs, depending on the number of PEVs, but it increased the residential area costs by 23 percent maximum. Thermal costs did not change because of the absence of an HP system. The total cost in this case study decreased by 7.8 percent. Moreover, for $C^{Con+DER}$, all costs decreased significantly, which shows the most favorable result among the case studies.

Table 5. The cost difference in comparison to the base case.

	$C^{Con+DER}$	C^{DER}	C^{Con}
Cost—Subway	−78% to −86%	0%	−35.7% to −50%
Cost—District	−36% to −40%	−51% to −53.6%	15% to 23%
Cost—Thermal	−94% to −96%	−94% to −95%	0%
Total Cost	−31%	−16.6%	−7.8%

SW costs decreased by up to 86 percent. Residential and thermal costs decreased by 40 and 96%, respectively. Finally, the total cost in this case showed a 31 percent decrease compared to the base case. Figure 8 illustrates the operation of an SWS interconnected with 25 PEVs on a typical day. It can be observed that approximately 86 percent of the total RBE has been charged back into the SWS, which results in an 86 percent cost reduction in the SWS, as presented in Table 5. The rest of this RBE charges the PEV batteries.

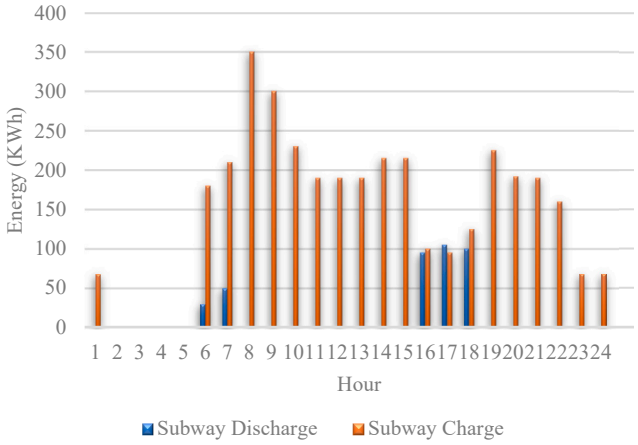

Figure 8. Operation of the SWS, when connected optimally to PEVs for the first scenario.

The results corresponding to the second PEV scenario, which assumed two PEV fleets, are shown in Figure 9. In this scenario, similar to the previous scenario, the total cost decreases in C^{Con} compared to the base case. In C^{DER} the total cost is further decreased from EUR 38.4 million to EUR 32 million when considering the fleet that contains 40 PEVs. Finally, $C^{Con+DER}$ shows a significant 31 percent decrease compared to the base case.

Figure 10 illustrates the operation of the PEVs, SWS, and DER technologies on a typical summer day considering $C^{Con+DER}$ for the second scenario. Similar to the previous scenario, the batteries charge during the peak PV power production period and discharge at other times. The operation of the SWS and the PEV fleet on a typical day is illustrated in Figure 11. Notably, almost 93 percent of the RBE has been charged back into the SWS, which is higher than the previous scenario. This is because, according to Table 1, the fleet is not present in the SW parking during the hours when the exchange between the SWS and the PEVs is beneficial, unlike the previous scenario.

This scenario further validates the outcomes of the case studies and demonstrates the importance of both DER technologies and the simultaneous optimization of the SWS and PEVs in the SC context.

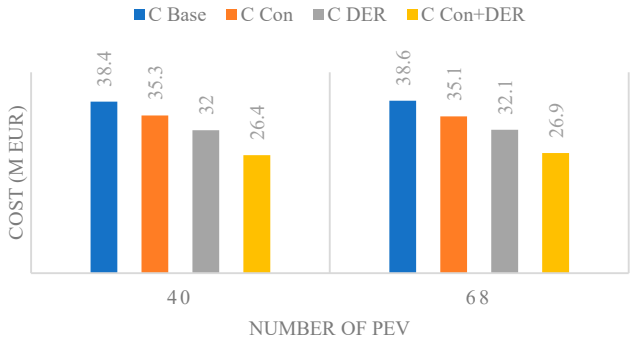

Figure 9. Total cost of each case study for different PEV numbers in the second PEV scenario.

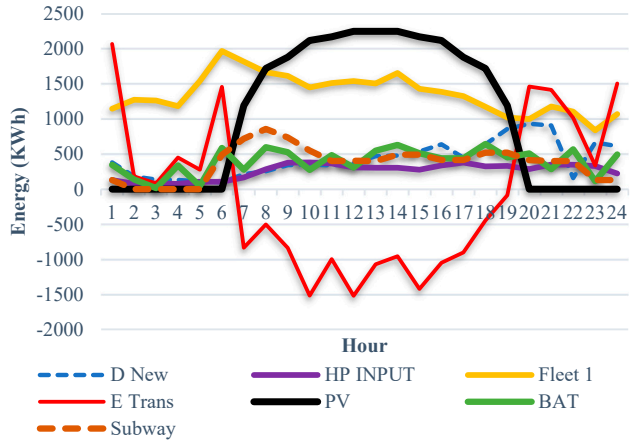

Figure 10. Daily operation of DER, PEV, and the SWS in summer for the second scenario.

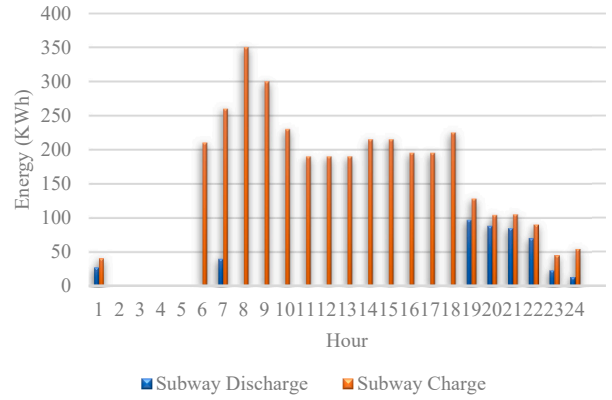

Figure 11. Operation of the SWS when connected optimally to PEVs for the second scenario.

5.2. Comparison

In this section, a comparison between different algorithms is presented to demonstrate the capability of the utilized i-GWOA compared to other algorithms including Genetic Algorithm (GA), hybrid Biogeography-Based Optimization and differential evolution (BBO-DE) algorithm, differential evolution algorithm (DE), particle swarm optimization (PSO) algorithm, and the simple GWOA. The optimal parameter settings of these algorithms that are utilized in this paper are presented in Table 6.

Tables 7–9 present the results for the first scenario with 25, 50, and 150 PEVs, respectively, calculated by different algorithms. The first two columns present the highest and the lowest costs calculated by each algorithm in all of the iterations. The average cost and the standard deviation for each algorithm are also presented in the next two columns. It is observed that the lowest cost for each scenario belongs to the i-GWOA. In addition,

the best, worst, and average costs calculated by the i-GWOA are the lowest among all of the algorithms. Also, the standard deviation of the costs computed for the i-GWOA is the lowest.

Table 6. Parameters of different algorithms.

Algorithm	Parameters
GA	Selection = roulette wheel, crossover = 0.8, Mutation m = 4
PSO	$w_{max}, w_{min}, w = \frac{iter}{iter\_maxmaxmax_{min}}$
DE	F = 0.2, cr = 0.6
BBO-DE	F = 0.2, cr = 0.6, KeepRate = 0.2, alpha = 0.9 Pmutation = 0.1, Sigma = 0.02 ∗ (Xmax − Xmin)
GWOA	a = 2 − 2 ∗ iter/iter_max
i-GWOA	a = 2 − 2 ∗ iter/iter_max

Table 7. Results obtained by different algorithms for 25 PEVs in the first scenario.

Solution Technique	Total Cost (Million EUR)			Standard Deviation (%)
	Best	Worst	Average	
GA	26.5	29	28.4	0.34
PSO	26	27.1	26.6	0.3
DE	25.7	26.6	26.1	0.21
BBO-DE	25.6	26.2	25.92	0.2
GWOA	25.7	26	25.75	0.15
i-GWOA	25.5	25.9	25.65	0.12

Table 8. Results obtained by different algorithms for 50 PEVs in the first scenario.

Solution Technique	Total Cost (Million EUR)			Standard Deviation (%)
	Best	Worst	Average	
GA	27	28.7	28.1	0.37
PSO	26.8	27.5	27.1	0.32
DE	26.3	27.1	26.6	0.2
BBO-DE	26.3	27.1	26.7	0.21
GWOA	26.1	26.7	26.4	0.13
i-GWOA	26	26.5	26.3	0.12

Table 9. Obtained results by different algorithms for 150 PEVs in the first scenario.

Solution Technique	Total Cost (Million EUR)			Standard Deviation (%)
	Best	Worst	Average	
GA	27.6	29.8	28.8	0.39
PSO	27.6	29.6	28.6	0.34
DE	27.4	28.2	27.9	0.22
BBO-DE	27.4	28.2	27.9	0.22
GWOA	27.1	27.8	27.5	0.16
i-GWOA	27	27.7	27.4	0.14

These results show the superiority of the i-GWOA and demonstrate that the i-GWOA is more accurate and more relevant than the other similar algorithms for solving the proposed problem.

6. Conclusions

The idea developed in this study was to demonstrate the impact of coordinated planning and operation of different segments in an SC and to model them to calculate the extent to which they affect the entire cost of the system. An iGW optimization algorithm was utilized to solve the optimization problem owing to the nonlinearities in the problem formulation.

In addition, the destruction cost of the batteries was added to the OF, and the energy losses relevant to the PV and HP systems were considered. Four different case studies in two PEV scenarios were conducted, and the results are discussed. The optimization algorithm showed good convenience by enhancing both the simulation runtime and numerical results compared with similar studies in the literature.

Four different case studies are considered in this paper to thoroughly demonstrate the impact of interconnections between PEVs and SWSs, along with the impacts of implementing various DERs in this model. In the first case, there is no interconnection between the PEVs and the SWS, and DERs are not considered. The second case study assesses the interconnection between PEVs and the SWS without considering DERs. In the third case study, DERs were considered, but the PEVs and SWS were optimized separately. Finally, in the fourth case study, both DER technologies and the connection between PEVs and SWSs were considered. In the first scenario, the entire cost is 37.2 Million Euro when 25 PEVs are considered. The entire cost gradually rises when the number of PEVs increases. This growth was caused by increasing the PEV loads, as the other costs remained the same. In addition, the SWS remains the same because no interconnection is considered. In the second case study, the entire cost was lower than the first case. This is caused by a decrease in SWS costs because of the interconnection, and thus, the SWS is able to take advantage of the higher storage capacity provided by PEVs. For the third case study, although the SW costs are the same as in the base case, and the investment costs are higher, it can be noted that the entire cost is lower than in the previous cases. This occurred as a consequence of the electrical and thermal generation of PV and HP, respectively, resulting in less energy being bought from the grid, in addition to load shifting being considered. Finally, in the fourth case study, where both the interconnection and presence of DER technologies are considered, the total cost shows a significant decrease.

The obtained results validate the benefits of interconnections between PEVs and SWSs and utilizing DER technologies in an SC model. However, many areas of this work can be developed in the future. One of these areas is considering further DER technologies, such as wind turbines, to completely model an SC. Another area that can be developed is the modeling of the uncertainties that can arise in the model, such as the behavior of PEVs, DER power output, and residential loads. To complete the discussion of the SC, the SC model can be completed by considering water desalination, as well as discussions related to cyber security and artificial intelligence to predict energy prices and network and subway loads. Also, the proposed system can be solved in a multi-objective problem that considers cost and emission together to reduce costs and emissions. Furthermore, the cyber security issue and secure transmitted data in an SC is one of the interesting topics that can be considered.

Author Contributions: Conceptualization, data curation, formal analysis, software, investigation, resources and writing—original draft carried out by M.S., M.S.-K. and M.P.; project administration, supervision carried out by T.N.; validation performed by T.N., E.S. and M.D.; writing—review and editing, visualization, methodology, and funding acquisition carried out by T.N., G.J., E.S. and M.D. All authors contributed equally to this paper. This research paper is contributed by the authors mentioned above. All authors have read and agreed to the published version of the manuscript.

Funding: This research is funded by the Research Office at the University of South Florida, Sarasota-Manatee Campus, from the Pioneer and IRG Interdisciplinary Research Grants awarded to Ehsan Sheybani.

Data Availability Statement: The original contributions presented in the study are included in the article, further inquiries can be directed to the corresponding author.

Conflicts of Interest: Author Masoud Shokri was employed by the company Fars Regional Electric Company. The remaining authors declare that the research was conducted in the absence of any commercial or financial relationships that could be construed as a potential conflict of interest. The Fars Regional Electric Company had no role in the design of the study; in the collection, analyses, or interpretation of data; in the writing of the manuscript, or in the decision to publish the results.

Nomenclature

Sets and Indices

m	Months
m_s	Months of summer
m_w	Months of winter
y	Years
v	Type of EVs
N_f	Number of fleets
N_s	Number of substations
q	Type of buildings
h	Hours

Parameters

C_{EV}	Maximum capacity of PEVs (kWh)
$Cap_{v,h}^{MaxEV}$	Maximum available capacity of PEVs (kWh)
$Cost_{ins}^{PV}$	Cost of installed PV (EUR/MW)
$Cost_{ins}^{HP}$	Cost of installed HP (EUR/MW)
$Cost_{ins}^{Bat}$	Upfront cost of stationary batteries (EUR/MW)
$Cost_{eq}^{ls}$	Cost of load shedding equipment (EUR/customer)
Day_m	Number of considered days in month m
$D_{q,m}^{Th}$	Total thermal demand (MWh)
D_h^{normTh}	Normalized residential thermal demand profile (%)
$EBuy_{m,h}^{com}$	Electricity base commercial price (EUR/kWh)
$EBuy_{m,h}^{res}$	Electricity base residential price (EUR/kWh)
$ECost_y^{inc}$	Annual growth of electricity base buy price (%)
$ESell_{m,h}$	Electricity base selling price (EUR/kWh)
n_{span}	Lifespan of PV and HP
n_{house}	Number equivalent customers per house
n_{EV}	Number of PEV user types
OM_{annual}^{HP}	Annual operation and maintenance of HP (EUR/MW)
OM_{annual}^{PV}	Annual operation and maintenance of PV (EUR/MW)
$\overline{P_{v,m,h}^{EVch}}/\underline{P_{v,m,h}^{EVch}}$	Max/min limits of energy charged into PEV (MWh)
$\overline{P_{v,m,h}^{EVdis}}/\underline{P_{v,m,h}^{EVdis}}$	Max/min limits of energy discharged from the PEV (MWh)
$\overline{P_{v,m,h}^{Subch}}/\underline{P_{v,m,h}^{Subch}}$	Max/min limits of energy charged from PEV into subway system (SWS) (MWh)
$\overline{P_{v,m,h}^{Subdis}}/\underline{P_{v,m,h}^{Subdis}}$	Max/min limits of energy discharged from SWS to PEV (MWh)
RB_h^{Sub}	Regenerative braking energy (MWh)
$SOC_{v,h}^{arrive}$	SOC of arriving PEV (%)
$SOC_{v,h}^{minEV}$	minimum SOC required for PEVs (%)
$Tariff^E$	Annual tariff for residential electric power (EUR/kW)
$Tariff^T$	Annual tariff for residential thermal power (EUR/customer)
$Tariff_{sub}^{peak}$	Annual tariff for SWS power at peak hours (EUR/kW)
$Tariff_{sub}^{mid}$	Annual tariff for SWS power at mid-peak hours (EUR/kW)
$Tariff_{sub}^{off}$	Annual tariff for SWS power at off-peak hours (EUR/kW)
$TCost_y^{inc}$	Annual growth of thermal energy buy price (%)
η_C^{EV}/η_D^{EV}	Charge/discharge efficiency of PEV battery (%)
$\eta_C^{sub}/\eta_D^{sub}$	Charge/discharge efficiency of SWS (%)
η_{energy}	Energy savings due to efficiency measures (%)
$loss^{HP}$	Total losses of HP system (%)
$loss^{PV}$	Total losses of PV system (%)
C_{HP}	HP coefficient of performance
$\Omega_{m,h}$	Global horizontal irradiance (W/m^2)

Variables

$Cost^{E}_{dist}$	Electric energy cost for the residential area (EUR)
$Cost^{P}_{dist}$	Electric power cost for the residential area (EUR)
$Cost^{E}_{sub}$	Electric energy cost for the SWS (EUR)
$Cost^{P}_{sub}$	Electric power cost for the SWS (EUR)
$Cost^{ETh}$	Thermal energy cost for the residential area (EUR)
$Cost^{pTh}$	Thermal power cost for the residential area (EUR)
$Cost^{PV}_{inv\&OM}$	Investments, operation, and maintenance costs of PV (EUR)
$Cost^{HP}_{inv\&OM}$	Investments, operation, and maintenance costs of HP (EUR)
$Cost^{Bat}_{inv}$	Investment cost of stationary batteries (EUR)
$Cost^{EV}_{inv}$	Investment cost of PEV batteries (EUR)
$Cost^{EV}_{op}$	Cost of aggregated PEVs (EUR)
$Cost^{EV}_{deg}$	Destruction cost of PEV batteries (EUR)
$Cost^{EV}_{pow}$	Operation cost of PEVs (EUR)
$Cost^{DR}_{eq}$	Investment cost of demand response equipment (EUR)
Cap^{Bat}_{q}	Stationary batteries capacity (MWh)
Cap^{HP}_{q}	HP capacity (MW)
Cap^{PV}_{q}	PV capacity (MW)
C_{h}	Hourly vehicle-to-grid price (EUR)
$P^{EV}_{v,h}$	Charge/discharge power rate of PEV fleet v at hour h
$D^{New}_{q,m,h}$	Consumption curve after profile change (MWh)
$D^{Sub}_{m,h}$	SWS consumption curve after profile change (MWh)
$E^{Grid}_{m,h}$	Grid energy transaction (MWh)
$E^{Trans}_{q,m,h}$	Energy transaction to the grid in each node (MWh)
$P^{BuyGrid}_{m,h}$	Entire energy bought from the grid (MWh)
$P^{SellGrid}_{m,h}$	Entire energy sold to the grid (MWh)
$P^{ThBuy}_{q,m}$	Thermal energy bought from the utility (MWh)
$P^{EContract}$	Annual contracted power (MW)
$P^{BatDis}_{q,m,h}$	Discharged energy of battery (MWh)
$P^{BatCh}_{q,m,h}$	Charged energy of battery (MWh)
$P^{EVdis}_{v,m,h}$	Discharged energy from PEV (MWh)
$P^{EVch}_{v,m,h}$	Energy charged into PEV (MWh)
$P^{Subdis}_{v,m,h}$	Energy discharged from the SWS to the PEV (MWh)
$P^{Subch}_{v,m,h}$	Energy charged from PEV into the SWS (MWh)
$P^{HP}_{q,m,h}$	HP thermal energy production (MWh)
$P^{inHP}_{q,m,h}$	HP input electricity (MWh)
$P^{PV}_{q,m,h}$	PV power production (MWh)
P^{off}_{sub}	Annual contracted power for the SWS during off-peak hours (MW)
P^{mid}_{sub}	Annual contracted power for the SWS during mid-peak hours (MW)
P^{peak}_{sub}	Contracted annual power for the SWS during peak hours (MW)
$SOC^{Bat}_{q,m,h}$	State of charge of battery (MWh)
$SOC^{EV}_{v,m,h}$	State of charge of PEV (MWh)
$U^{EV}_{v,m,h}$	Binary variables for on-grid PEVs
$U^{EVch}_{v,m,h}/U^{EVdis}_{v,m,h}$	Binary variables for charge/discharge of PEVs
$U^{Sub}_{v,m,h}$	Binary variables for SWS connection of PEVs
$U^{Subch}_{v,m,h}/U^{Subdis}_{v,m,h}$	Binary variables for charge/discharge of PEVs in connection with the SWS

References

1. Kumar, P.; Nikolovski, S.; Ali, I.; Thomas, M.S.; Ahuja, H. Impact of Electric Vehicles on Energy Efficiency with Energy Boosters in Coordination for Sustainable Energy in Smart Cities. *Processes* **2022**, *10*, 1593. [CrossRef]
2. Parra-Domínguez, J.; López-Blanco, R.; Pinto-Santos, F. Approach to the Technical Processes of Incorporating Sustainability Information—The Case of a Smart City and the Monitoring of the Sustainable Development Goals. *Processes* **2022**, *10*, 1651. [CrossRef]

3. Shokri, M.; Niknam, T.; Mohammadi, M.; Dehghani, M.; Siano, P.; Ouahada, K.; Sarvarizade-Kouhpaye, M. A Novel Stochastic Framework for Optimal Scheduling of Smart Cities as an Energy Hub. *IET Gener. Transm. Distrib.* **2024**, *18*, 2421–2434. [CrossRef]
4. Jokar, H.; Niknam, T.; Dehghani, M.; Sheybani, E.; Pourbehzadi, M.; Javidi, G. Efficient Microgrid Management with Meerkat Optimization for Energy Storage, Renewables, Hydrogen Storage, Demand Response, and EV Charging. *Energies* **2023**, *17*, 25. [CrossRef]
5. Amamra, S.A.; Marco, J. Vehicle-to-grid aggregator to support power grid and reduce electric vehicle charging cost. *IEEE Access* **2019**, *7*, 178528–178538. [CrossRef]
6. Shi, D.; Li, S.; Liu, K.; Wang, Y.; Liu, R.; Guo, J. Adaptive energy management strategy based on intelligent prediction of driving cycle for plug− in hybrid electric vehicle. *Processes* **2022**, *10*, 1831. [CrossRef]
7. Mehta, R.; Verma, P.; Srinivasan, D.; Yang, J. Double-layered intelligent energy management for optimal integration of plug-in electric vehicles into distribution systems. *Appl. Energy* **2019**, *233*, 146–155. [CrossRef]
8. Liu, H.; Zhou, M.; Guo, X.; Zhang, Z.; Ning, B.; Tang, T. Timetable optimization for regenerative energy utilization in subway systems. *IEEE Trans. Intell. Transp. Syst.* **2018**, *20*, 3247–3257. [CrossRef]
9. Wu, C.; Lu, S.; Xue, F.; Jiang, L.; Chen, M.; Yang, J. A two-step method for energy-efficient train operation, timetabling, and onboard energy storage device management. *IEEE Trans. Transp. Electrif.* **2021**, *7*, 1822–1833. [CrossRef]
10. Khodaparastan, M.; Mohamed, A. A study on super capacitor wayside connection for energy recuperation in electric rail systems. In Proceedings of the 2017 IEEE Power & Energy Society General Meeting, Chicago, IL, USA, 16–20 July 2017; pp. 1–5.
11. Roch-Dupré, D.; Cucala, A.P.; Pecharromán, R.R.; López-López, Á.J.; Fernández-Cardador, A. Evaluation of the impact that the traffic model used in railway electrical simulation has on the assessment of the installation of a Reversible Substation. *Int. J. Electr. Power Energy Syst.* **2018**, *102*, 201–210. [CrossRef]
12. Al-Refaie, A.; Lepkova, N. Satisfaction with Rooftop Photovoltaic Systems and Feed-in-Tariffs Effects on Energy and Environmental Goals in Jordan. *Processes* **2024**, *12*, 1175. [CrossRef]
13. Calvillo, C.F.; Turner, K.; Bell, K.; McGregor, P. Impacts of residential energy efficiency and electrification of heating on energy market prices. In Proceedings of the 15th IAEE European Conference, Vienna, Austria, 3–6 September 2017.
14. Calvillo, C.F.; Sánchez-Miralles, Á.; Villar, J. Synergies of electric urban transport systems and distributed energy resources in smart cities. *IEEE Trans. Intell. Transp. Syst.* **2017**, *19*, 2445–2453. [CrossRef]
15. Jafari, M.; Kavousi-Fard, A.; Niknam, T.; Avatefipour, O. Stochastic synergies of urban transportation system and smart grid in smart cities considering V2G and V2S concepts. *Energy* **2021**, *215*, 119054. [CrossRef]
16. Papari, B.; Edrington, C.S.; Ozkan, G.; Bader, P.R. Stochastic analysis of regenerative braking energy of urban transportation system associated with Plug-in electrical vehicle in smart city. In Proceedings of the 2021 IEEE Fourth International Conference on DC Microgrids (ICDCM), Arlington, VA, USA, 18–21 July 2021; pp. 1–5.
17. Zhang, L.; Cheng, L.; Alsokhiry, F.; Mohamed, M.A. A novel stochastic blockchain-based energy management in smart cities using V2S and V2G. *IEEE Trans. Intell. Transp. Syst.* **2022**, *24*, 915–922. [CrossRef]
18. Niknam, T.; Azizipanah-Abarghooee, R.; Narimani, M.R. Reserve constrained dynamic optimal power flow subject to valve-point effects, prohibited zones and multi-fuel constraints. *Energy* **2012**, *47*, 451–464. [CrossRef]
19. Talbi, E.G. *Metaheuristics: From Design to Implementation*; John Wiley & Sons: Hoboken, NJ, USA, 2009.
20. Nadimi-Shahraki, M.H.; Taghian, S.; Mirjalili, S. An improved grey wolf optimizer for solving engineering problems. *Expert Syst. Appl.* **2021**, *166*, 113917. [CrossRef]
21. Rojek, I.; Mikołajewski, D.; Mroziński, A.; Macko, M. Machine Learning-and Artificial Intelligence-Derived Prediction for Home Smart Energy Systems with PV Installation and Battery Energy Storage. *Energies* **2023**, *16*, 6613. [CrossRef]
22. Maisel, F.; Neef, C.; Marscheider-Weidemann, F.; Nissen, N.F. A forecast on future raw material demand and recycling potential of lithium-ion batteries in electric vehicles. *Resour. Conserv. Recycl.* **2023**, *192*, 106920. [CrossRef]
23. Fernández, I.J.; Calvillo, C.F.; Sánchez-Miralles, A.; Boal, J. Capacity fade and aging models for electric batteries and optimal charging strategy for electric vehicles. *Energy* **2013**, *60*, 35–43. [CrossRef]
24. Zendehboudi, A. Energy, exergy, and exergoeconomic analyses of an air source transcritical CO_2 heat pump for simultaneous domestic hot water and space heating. *Energy* **2024**, *290*, 130295. [CrossRef]
25. Yang, Y.; Wang, Y.; Xu, Z.; Xie, B.; Hu, Y.; Yu, J.; Chen, Y.; Zhang, T.; Lu, Z.; Gong, Y. Performance Comparison of High-Temperature Heat Pumps with Different Vapor Refrigerant Injection Techniques. *Processes* **2024**, *12*, 566. [CrossRef]
26. Awad, M.; Said, A.; Saad, M.H.; Farouk, A.; Mahmoud, M.M.; Alshammari, M.S.; Alghaythi, M.L.; Aleem, S.H.; Abdelaziz, A.Y.; Omar, A.I. A review of water electrolysis for green hydrogen generation considering PV/wind/hybrid/hydropower/geothermal/tidal and wave/biogas energy systems, economic analysis, and its application. *Alex. Eng. J.* **2024**, *87*, 213–239. [CrossRef]
27. Gupta, S.; Maulik, A.; Das, D.; Singh, A. Coordinated stochastic optimal energy management of grid-connected microgrids considering demand response, plug-in hybrid electric vehicles, and smart transformers. *Renew. Sustain. Energy Rev.* **2022**, *155*, 111861. [CrossRef]
28. Ahmed, I.; Rehan, M.; Basit, A.; Tufail, M.; Hong, K.S. A dynamic optimal scheduling strategy for multi-charging scenarios of plug-in-electric vehicles over a smart grid. *IEEE Access* **2023**, *11*, 28992–29008. [CrossRef]
29. Yin, Z.; Ma, X.; Su, R.; Huang, Z.; Zhang, C. Regenerative braking of electric vehicles based on fuzzy control strategy. *Processes* **2023**, *11*, 2985. [CrossRef]

30. Calvillo, C.F.; Sánchez-Miralles, A.; Villar, J.; Martín, F. Impact of EV penetration in the interconnected urban environment of a smart city. *Energy* **2017**, *141*, 2218–2233. [CrossRef]
31. Akil, M.; Dokur, E.; Bayindir, R. The SOC based dynamic charging coordination of EVs in the PV-penetrated distribution network using real-world data. *Energies* **2021**, *14*, 8508. [CrossRef]
32. Chevrolet Pressroom—United States—Spark EV. Available online: https://media.gm.com/content/media/us/en/chevrolet/vehicles/spark-ev/2016.html (accessed on 1 June 2019).
33. Chinchilla, M.; Santos-Martin, D.; Carpintero-Renteria, M.; Lemon, S. Worldwide annual optimum tilt angle model for solar collectors and photovoltaic systems in the absence of site meteorological data. *Appl. Energy* **2021**, *281*, 116056. [CrossRef]
34. Fan, S.; Wang, Y.; Cao, S.; Sun, T.; Liu, P. A novel method for analyzing the effect of dust accumulation on energy efficiency loss in photovoltaic (PV) system. *Energy* **2021**, *234*, 121112. [CrossRef]
35. How Much Do Smart Meters Cost? Available online: https://www.siemens.com/global/en/company/stories/infrastructure/2022/tata-power-smart-meter-data-management.html (accessed on 3 May 2022).
36. Calvillo, C.F.; Sánchez-Miralles, Á.; Villar, J. Price-maker optimal planning and operation of distributed energy resources. In Proceedings of the 2016 13th International Conference on the European Energy Market (EEM), Porto, Portugal, 6–9 June 2016; pp. 1–5.
37. Iberdrola. Residential Time-of-Use Electric Tariff. Available online: https://www.iberdrola.es/home/electricity (accessed on 1 September 2019).
38. Iberdrola. Residential Gas Tariff. Available online: https://www.iberdrola.es/home/gas/home-gas-plan (accessed on 18 April 2017).